A simple dynamic subgrid-scale model for LES of particle-laden turbulence

George Ilhwan Park, Maxime Bassenne, Javier Urzay,[*] and Parviz Moin

Center for Turbulence Research, Stanford University, Stanford, California 94305-3024, USA

(Received 1 July 2016; published 14 April 2017)

In this study, a dynamic model for large-eddy simulations is proposed in order to describe the motion of small inertial particles in turbulent flows. The model is simple, involves no significant computational overhead, contains no adjustable parameters, and is flexible enough to be deployed in any type of flow solvers and grids, including unstructured setups. The approach is based on the use of elliptic differential filters to model the subgrid-scale velocity. The only model parameter, which is related to the nominal filter width, is determined dynamically by imposing consistency constraints on the estimated subgrid energetics. The performance of the model is tested in large-eddy simulations of homogeneous-isotropic turbulence laden with particles, where improved agreement with direct numerical simulation results is observed in the dispersed-phase statistics, including particle acceleration, local carrier-phase velocity, and preferential-concentration metrics.

I. INTRODUCTION

In Lagrangian descriptions of turbulent flows laden with heavy particles, such as liquid droplets or solid particles whose density is much larger than that of the carrier fluid, the dispersed phase is described by the equation of the trajectory

$$\frac{dx_{p,i}}{dt} = u_{p,i} \tag{1}$$

and the equation of motion

$$\frac{4}{3}\pi\rho_p a^3 \frac{du_{p,i}}{dt} = 6\pi\mu a(u_i - u_{p,i}), \tag{2}$$

where it is additionally assumed that the particles are sufficiently small such that the flow in their vicinity is dominated by molecular transport. In this formulation, $x_{p,i}$ and $u_{p,i}$ are the particle position and particle velocity, respectively, ρ_p and a are the particle density and radius, respectively, and μ is the dynamic viscosity of the carrier phase. In Eq. (2), u_i refers to the velocity of the carrier phase interpolated at the particle position. Ideally, u_i is obtained from costly direct numerical simulations (DNS) to retain all scales of the fluid motion influencing the dynamics of particles. In contrast, in large-eddy simulations (LES) the only velocity available is low-pass filtered, denoted here by $\overline{u}_i$. In particular, when the mass of particles per unit mass of carrier phase is small, the filtered velocity is obtained by integrating

$$\frac{\partial\overline{u}_i}{\partial x_i} = 0 \tag{3}$$

and

$$\frac{\partial\overline{u}_i}{\partial t} + \overline{u}_j\frac{\partial\overline{u}_i}{\partial x_j} = -\frac{1}{\rho}\frac{\partial\overline{p}}{\partial x_i} + \nu\frac{\partial^2\overline{u}_i}{\partial x_j\partial x_j} - \frac{\partial\mathcal{T}_{ij}^{\text{LES}}}{\partial x_j}, \tag{4}$$

which represent, respectively, the filtered equations of mass and momentum conservation for an incompressible flow. In Eq. (4), $\overline{p}$ is the hydrodynamic pressure, ν is the kinematic viscosity, and ρ is the carrier-phase density, with $\rho/\rho_p \ll 1$ in most practical applications [1]. The symbol $\mathcal{T}_{ij}^{\text{LES}} = \overline{u_i u_j} - \overline{u}_i\overline{u}_j$ denotes the subgrid-scale (SGS) stress tensor for the carrier phase.

---

[*]Corresponding author: jurzay@stanford.edu

The utilization of $\overline{u}_i$ in Eq. (2) in place of the unfiltered velocity u_i leads to inaccurate results when the particles are sufficiently light to interact with the unresolved eddies. Expressed in dimensionless form, the regime where these interactions are important is [2]

$$\text{St}_{\text{SGS}} = t_a/t_\Delta \lesssim 1, \tag{5}$$

where St_{SGS} is an SGS Stokes number based on the characteristic particle-relaxation time $t_a = (2/9)(\rho_p/\rho)a^2/\nu$ and the cutoff fluctuation time t_Δ introduced by the eddies whose size is of the same order as the grid size Δ. In general, t_Δ is a time scale measured in the reference frame of the particle. In conditions where (5) is satisfied, the particles become tracers of the large eddies and the cutoff fluctuation time can be approximated from Kolmogorov scaling as $t_\Delta \sim (\Delta^2/\epsilon)^{1/3}$, where ϵ is the mean dissipation.

In this study, the focus is on LES of turbulent flows in which the particles interact with the unresolved eddies so that condition (5) is satisfied. In this limit, unless an SGS model is employed to model the subgrid velocity fluctuations $u_i' = u_i - \overline{u}_i$ in Eq. (2), the effective maximum value of the Stokes number based on the smallest resolved scale becomes that given by St_{SGS}, which is, by definition, smaller than the Stokes number based on the Kolmogorov scales. The absence of small scales in LES, along with their associated intermittency, has negative consequences on the prediction of a number of metrics for the dispersed phase such as relative dispersion, collision rates, preferential concentration, turbophoresis, and particle-acceleration statistics [2–9].

A number of previous investigations have addressed this issue by proposing closure models for the SGS velocity u_i'. These could be grouped into four different categories: stochastic [10–20], approximate deconvolution (AD) [21,22], hybrid combinations of the two [23], and kinematic-simulation (KS) [24–26] models. The four types of models share the common goal of palliating the deficit of small scales in LES. For instance, stochastic models typically employ a fluctuation velocity obtained from the solution of a Langevin equation supplemented with a random source, which is responsible for providing the high-frequency forces exerted by the unresolved eddies on the particles in the Lagrangian reference frame. However, stochastic models are known to miscalculate preferential concentration since they are generally dispersive at all Stokes numbers [20]. Additionally, stochastic models generally require parameter calibration, with the exception of a relevant approach in Ref. [14] in which the model parameter is obtained from a condition of consistency with the SGS kinetic energy, but without taking into account particle inertia. Approximate-deconvolution models, on the other hand, calculate the unfiltered velocity u_i in Eq. (2) by approximate deconvolution of the resolved velocity $\overline{u}_i$, which requires the utilization of series expansions for filter inversion along with an *ad hoc* choice of the test-filter level and calibration of the effective filter width. This broad category includes scale-similarity models of SGS velocity estimation [27–29].

The model investigated in this study belongs to the AD family. However, the filter chosen in this study is exactly invertible and the effective filter width is computed dynamically with no tuning of parameters being required. Approximate-deconvolution models tend to outperform stochastic models in predicting preferential concentration, although they underpredict particle acceleration because of the intrinsic limitations of the deconvolution method in injecting disturbances of frequencies higher than those of the resolved eddies. Hybrid approaches correspond to blended combinations of stochastic and AD models that extend the range of performance of each separate type of model. Lastly, KS models aim at spectrally regenerating the missing scales of turbulence by incorporating high-wavenumber modes in the velocity field. Despite their higher computational cost, KS models are perhaps the most promising approach for predicting preferential concentration, since this phenomenon is caused by the intermittency of the vorticity and strain-rate fields at scales beyond the grid cutoff wavenumber. However, the coarser the LES grid is, the more difficult it is to regenerate eddies at the missing scales, since they become increasingly more anisotropic and problem dependent. In fact, the problem at hand in this investigation, namely, the one in which particles interact with SGS turbulent eddies and preferentially concentrate, is a challenging one that puts traditional LES models to the test, in that the fine scale features of the flow field, rather than the structures resolved by the grid, play a major role in the relevant dispersed-phase dynamics.

The objective of this investigation is to formulate and test a model for the SGS velocity of the carrier phase u_i', which, in conjunction with the filtered velocity $\overline{u}_i$, leads to an estimate of the unfiltered velocity u_i that is used to integrate the particle equation of motion (2). The proposed model is based on differential filters [30–34] and employs a dynamic procedure to determine the value of an otherwise adjustable parameter. Using this model, LES of dilute particle-laden homogeneous-isotropic turbulence are performed that show improved agreement with DNS results in terms of dispersed-phase statistics, including local carrier-phase velocity sampled by particles, particle acceleration, and preferential-concentration metrics. Tests of the model in two-way coupled flows are deferred to future work, although brief comments on potential impacts of the present approach in those flows are provided.

The rest of this article is structured as follows. The formulation of the SGS model is given in Sec. II. The dynamic procedures for the model parameter are described in Sec. III. The performance of the model is addressed in Sec. IV. Finally, concluding remarks and future prospectives are provided in Sec. V.

II. SUBGRID-SCALE MODEL (LES DIFFERENTIAL-FILTER MODEL)

The SGS model for particles proposed here, referred to as the differential-filter (DF) model, is based on computing the velocity u_i in Eq. (2) using the filtered one $\overline{u}_i$ according to the expression

$$u_i = \overline{u}_i - \frac{\partial}{\partial x_j}\left(b^2 \frac{\partial \overline{u}_i}{\partial x_j}\right). \tag{6}$$

The corresponding SGS velocity component is simply given by

$$u_i' = u_i - \overline{u}_i = \frac{\partial}{\partial x_j}\left(b^2 \frac{\partial \overline{u}_i}{\partial x_j}\right). \tag{7}$$

Equation (6) represents the definition of an elliptic differential filter [30–34]. In this formulation, b is a model parameter that is of the same order as the LES grid spacing Δ and controls the nominal filter width. In principle, there are no restrictions related to the spatial variability of b. If b is spatially uniform, then the filtered velocity

$$\overline{u}_i(\mathbf{x},t) = \int_{\mathbf{x}'} u_i(\mathbf{x}',t)G(\mathbf{x},\mathbf{x}')d^3\mathbf{x}' \tag{8}$$

can be expressed in terms of an exponentially decaying filter kernel

$$G(\mathbf{x},\mathbf{x}') = \frac{\exp\{-|\mathbf{x}-\mathbf{x}'|/b\}}{4\pi b^2|\mathbf{x}-\mathbf{x}'|} \tag{9}$$

that corresponds to the Green's function of Eq. (6), with $\mathbf{x}$ indicating a position vector. In all cases, the model parameter b can be computed dynamically, as described in Sec. III. Note that Eq. (6) guarantees that the volume-averaged values of u_i and $\overline{u}_i$ are the same in triply-periodic domains or in bounded domains where $b \to 0$ at the boundaries.

The utilization of LES for the carrier phase, in conjunction with the DF-modeled velocity (6) for integrating the particle equation of motion (2), is referred to as the LES-DF model in what follows. In the LES-DF model, at each time step the velocity u_i computed using (6) is employed in integrating the equation of motion (2) for the particles. Remarkably, the numerical operations involved in the model can easily be done with any type of flow solver and grid at low cost, including unstructured grids. On the other hand, the acronym LES will be used to refer to LES performed by replacing u_i by $\overline{u}_i$ in the particle equation of motion (2), thereby neglecting the effect of the subgrid scales on the dispersed-phase dynamics.

It is instructive to analyze the statistics of the LES-DF velocity field. Figure 1 shows that for homogeneous-isotropic flows (described in Sec. IV) the Fourier spectra of kinetic energy and enstrophy in the LES-DF model are intensified with respect to those of LES near the grid cutoff. On
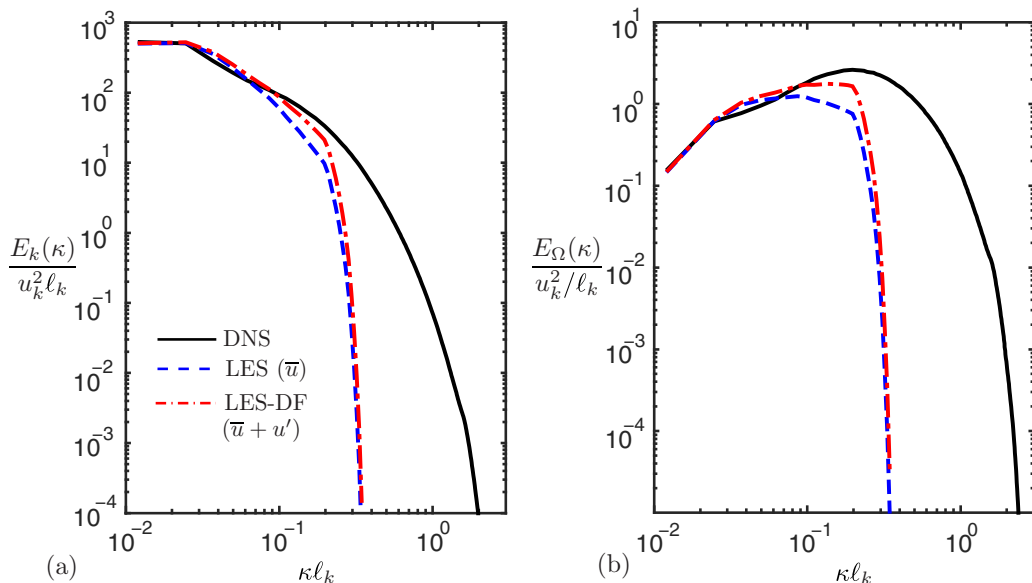
FIG. 1. Ensemble-averaged spectra for (a) turbulent kinetic energy and (b) enstrophy in homogeneous-isotropic turbulence as a function of the wavenumber κ, corresponding to DNS (256^3 grid points), LES (32^3 grid points), and the LES-DF model (32^3 grid points) at Re$_\lambda = 85$. The DF-model constant b is spatially uniform and is obtained using the dynamic procedure described in Sec. III B. The symbols Re$_\lambda$, ℓ_k and u_k denote, respectively, the Taylor-Reynolds number and the length and turnover velocity of the Kolmogorov eddies. Further details about the computational setup are provided in Sec. IV.

the other hand, at small wavenumbers, the effect of the DF model vanishes and the LES-DF spectra approach those of LES. These dynamics are easily explained by transforming Eq. (6) into Fourier space, which indicates that the DF-modeled velocity spectrum is $1 + b^2\kappa^2$ times the resolved one when b is spatially uniform, with κ the wavenumber modulus.

The energization of the near-cutoff scales in the LES-DF model is accompanied with an increase in intermittency of the velocity gradients. This is observed in Fig. 2, which shows that the tails of the probability density function (PDF) of the LES-DF velocity gradients become wider than those of LES, with a corresponding increase in the flatness. The enhanced spatial intermittency of the near-cutoff scales caused by the DF-modeled subgrid velocity (7) is also observed in the cross-sectional contours shown in Fig. 3 for the same flow. However, it should be emphasized that the DF-modeled velocity u_i has the same wavenumber range of spectral content as the resolved velocity $\overline{u}_i$ and therefore it is not a full-scale quantity as in DNS. This implies that the intermittency of the small scales in the DNS is not fully recovered by the LES-DF model, as observed in Fig. 3 and quantified by the differences between DNS and LES-DF flatness coefficients of the velocity gradients in Fig. 2. Further implications of this deficit for particle-laden flows are discussed in Sec. IV.

In contrast to other types of filters that require arbitrary truncation of series expansions for inversion, the deconvolution operation made in the DF model (6) is formally exact. When expressed as $\overline{u}_i = u_i + b^2\partial^2\overline{u}_i/\partial x_j \partial x_j$, the filtered velocity is reminiscent of the first two terms in the series expansion of a box-filtered velocity [35], with the exception that here the Laplacian acts upon $\overline{u}_i$ instead of u_i. In this way, the DF model (6) could be interpreted as an approximate de-averaging of the resolved velocity. However, the DF model, along with the dynamic procedures described below for the coefficient b, do not exactly represent a de-averaging operation, but rather a more general deconvolution that satisfies consistency constraints on the subgrid energetics. The DF model (6) can
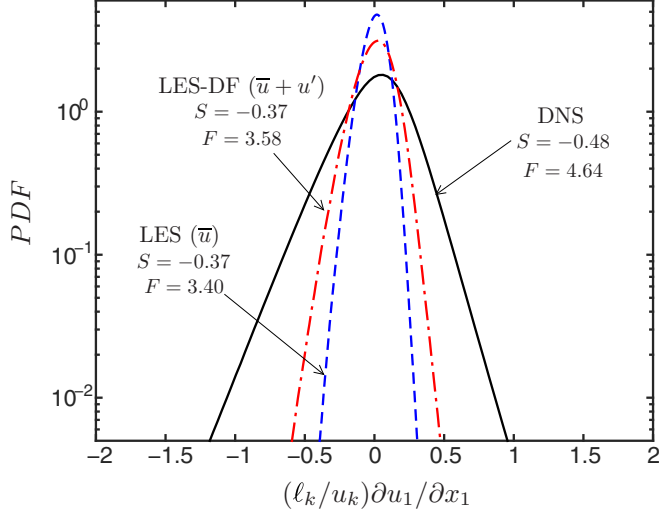
FIG. 2. Ensemble-averaged PDF of the velocity gradient $\partial u_1/\partial x_1$ in DNS (256^3 grid points), LES (32^3 grid points), and the LES-DF model (32^3 grid points) at $\mathrm{Re}_\lambda = 85$, including corresponding values of skewness S and flatness factors F. The DF-model constant b is spatially uniform and is obtained using the dynamic procedure described in Sec. III B.

be utilized for integrating the motion of mono- or polydisperse clouds of particles with arbitrary inertia. It acts dispersively or antidispersively depending on the value of the corresponding Stokes number of the particles (defined below) and can propagate information of large-scale local anisotropy into the subgrid scales.

In this study, an important approximation is made when using Eq. (6), namely, that $\overline{u}_i$ is the implicitly filtered velocity computed from LES using Eqs. (3) and (4), as opposed to being the one resulting from the solution of the Navier Stokes equations explicitly filtered with a differential filter for complete consistency. Unless explicit filtering is used [36], it is not warranted that the closure (6)
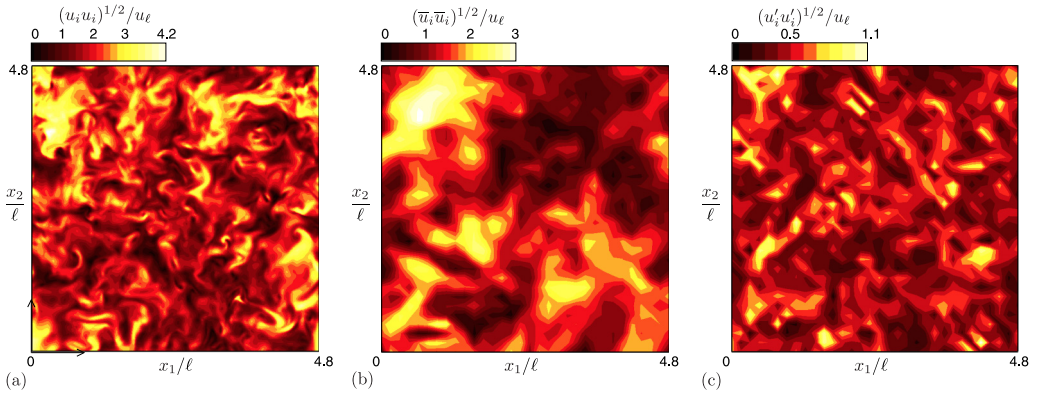

FIG. 3. Instantaneous midplane cross section of the contours of the velocity magnitude (solid contours) in homogeneous-isotropic turbulence at $\mathrm{Re}_\lambda = 85$. (a) DNS (256^3 grid points), (b) LES (32^3 grid points), and (c) DF-modeled subgrid velocity field in the LES-DF model (32^3 grid points). The symbols ℓ and u_ℓ denote, respectively, the integral length and velocity scales. The DF-model constant b is spatially uniform and is obtained using the dynamic procedure described in Sec. III B.

is fully consistent with the model for the SGS stress tensor $\mathcal{T}_{ij}^{\text{LES}}$ in Eq. (4). This inconsistency is palliated below with a dynamic procedure for the model parameter b in Eq. (6) that makes the DF model consistent with the energetics predicted by the model for the SGS stress tensor of the carrier phase $\mathcal{T}_{ij}^{\text{LES}}$.

III. DYNAMIC PROCEDURES FOR THE MODEL PARAMETER

Two dynamic procedures for computing the model parameter b are described in this section. As shown in Sec. IV, both procedures lead to similar results in the range of parameters considered here, with the one described in Sec. III B being consistently observed to produce better agreement with DNS results.

A. Dynamic procedure based on dissipation matching [LES-DF(ϵ) procedure]

The first dynamic procedure is referred to as LES-DF(ϵ) and imposes consistency between the SGS dissipation calculated from the model for the carrier-phase SGS stress tensor $\epsilon_{\text{SGS}}^{\text{LES}} = -\mathcal{T}_{ij}^{\text{LES}}\overline{S}_{ij}$ and the one obtained from the DF model for particles $\epsilon_{\text{SGS}}^{\text{DF}} = -\mathcal{T}_{ij}^{\text{DF}}\overline{S}_{ij}$, where $\overline{S}_{ij} = (1/2)(\partial\overline{u}_i/\partial x_j + \partial\overline{u}_j/\partial x_i)$ is the strain rate of the resolved velocity field and $\mathcal{T}_{ij}^{\text{DF}}$ is an SGS stress tensor directly obtained from the differential-filter formulation, as explained below. Note that a similar dynamic approach, albeit in a different model, has been used in an earlier work on SGS velocity estimation that yields improved results [37].

The description of the dynamic procedure begins by deriving an equation for the SGS stress tensor $\mathcal{T}_{ij}^{\text{DF}} = \overline{u_i u_j} - \overline{u}_i\overline{u}_j$. Recursive use of the differential-filter definition (6) for computing the expression

$$u_i u_j = \left[\overline{u}_i - \frac{\partial}{\partial x_k}\left(b^2\frac{\partial\overline{u}_i}{\partial x_k}\right)\right]\left[\overline{u}_j - \frac{\partial}{\partial x_m}\left(b^2\frac{\partial\overline{u}_j}{\partial x_m}\right)\right] \tag{10}$$

and subtracting it from

$$u_i u_j = \overline{u_i u_j} - \frac{\partial}{\partial x_k}\left(b^2\frac{\partial\overline{u_i u_j}}{\partial x_k}\right) \tag{11}$$

yields the partial differential equation

$$\mathcal{T}_{ij}^{\text{DF}} - \frac{\partial}{\partial x_k}\left(b^2\frac{\partial\mathcal{T}_{ij}^{\text{DF}}}{\partial x_k}\right) = R_{ij}, \tag{12}$$

with R_{ij} an auxiliary tensor given by

$$R_{ij} = 2b^2\frac{\partial\overline{u}_i}{\partial x_k}\frac{\partial\overline{u}_j}{\partial x_k} + \frac{\partial}{\partial x_n}\left(b^2\frac{\partial\overline{u}_i}{\partial x_n}\right)\frac{\partial}{\partial x_p}\left(b^2\frac{\partial\overline{u}_j}{\partial x_p}\right), \tag{13}$$

where the filtered velocities $\overline{u}_i$ are the LES resolved ones. A comparison of the differential-filter definition (6) with Eq. (12) leads to

$$\mathcal{T}_{ij}^{\text{DF}} = \overline{R}_{ij}, \tag{14}$$

where the overbar in $\overline{R}_{ij}$ refers to the differential-filter operator acting on R_{ij}.

The consistency condition between the SGS dissipations predicted by both models, $\epsilon_{\text{SGS}}^{\text{DF}} = \epsilon_{\text{SGS}}^{\text{LES}}$, can be expressed as

$$\mathcal{T}_{ij}^{\text{DF}}\bar{S}_{ij} = \mathcal{T}_{ij}^{\text{LES}}\bar{S}_{ij}. \tag{15}$$
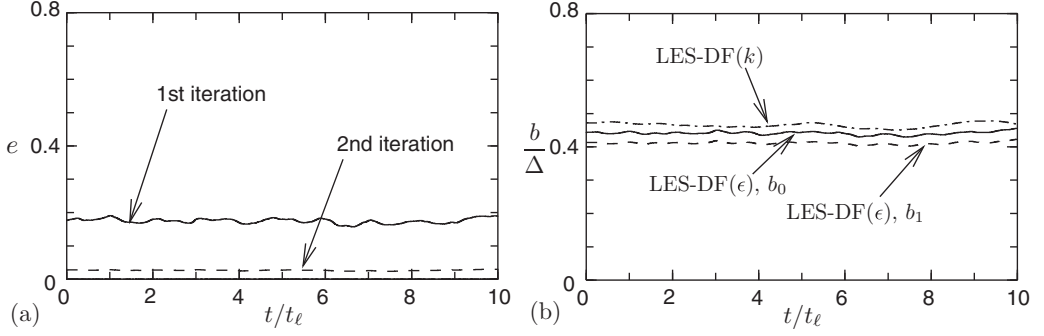
FIG. 4. Sample time histories of (a) the relative error e [Eq. (21)] using the dissipation-matching procedure and (b) the spatially uniform coefficient b determined dynamically from both procedures using Eqs. (17) and (23).

This consistency is enforced by multiplying Eq. (12) by $\bar{S}_{ij}$ and substituting Eq. (15) in the resulting expression, which gives

$$\mathcal{T}_{ij}^{\text{LES}}\overline{S}_{ij} - b^2 \frac{\partial^2 \mathcal{T}_{ij}^{\text{DF}}}{\partial x_k \partial x_k}\overline{S}_{ij} - 2b\frac{\partial b}{\partial x_m}\frac{\partial \mathcal{T}_{ij}^{\text{DF}}}{\partial x_m}\overline{S}_{ij} = R_{ij}\overline{S}_{ij}, \tag{16}$$

where R_{ij} is given in Eq. (13) and $\mathcal{T}_{ij}^{\text{DF}}$ is parametrized by the unknown b as in Eqs. (13) and (14).

Equation (16) represents a nonlinear partial differential equation whose solution b provides the local value of the model parameter. The simulations presented in this study, however, employ a spatially uniform b obtained by solving a much simpler volume-averaged version of Eq. (16), namely,

$$\langle \alpha_{ij}\bar{S}_{ij}\rangle b^4 + \langle \beta_{ij}\bar{S}_{ij}\rangle b^2 - \langle \mathcal{T}_{ij}^{\text{LES}}\bar{S}_{ij}\rangle = 0, \tag{17}$$

where the bracketed operator $\langle \cdot \rangle$ indicates volumetric averaging. This corresponds to enforcing the consistency condition (15) on volume average, which is particularly suitable for the present study focused on triply-periodic flows. In this formulation, α_{ij} and β_{ij} are given by

$$\alpha_{ij} = \frac{\partial^2 \overline{u}_i}{\partial x_k \partial x_k}\frac{\partial^2 \overline{u}_j}{\partial x_m \partial x_m}, \tag{18}$$

$$\beta_{ij} = 2\frac{\partial \overline{u}_i}{\partial x_\ell}\frac{\partial \overline{u}_j}{\partial x_\ell} + \frac{\partial^2 \mathcal{T}_{ij}^{\text{DF}}}{\partial x_k \partial x_k}. \tag{19}$$

The positive root $b^2 > 0$ of Eq. (17) corresponds to the physically relevant solution for the model parameter.

In principle, Eq. (17) is an implicit equation for the dynamic coefficient b that has to be solved iteratively at each time step, because the term involving $\mathcal{T}_{ij}^{\text{DF}}$ in β_{ij} depends on the unknown b. In order to reduce the associated computational cost, an approximate solution is to linearize the second term on the left-hand side of Eq. (17) by making

$$\left\langle \overline{S}_{ij}\frac{\partial^2 \mathcal{T}_{ij}^{\text{DF}}}{\partial x_k \partial x_k}\right\rangle \simeq \left\langle \overline{S}_{ij}\frac{\partial^2 \mathcal{T}_{ij}^{\text{LES}}}{\partial x_k \partial x_k}\right\rangle \tag{20}$$

which transforms Eq. (17) into a biquadratic equation where all terms are known. The positive root of this equation yields the first approximation b_0 to the dynamic coefficient. Figure 4(a) shows that this simplification leads to a relative error

$$e = \langle \epsilon_{\text{SGS}}^{\text{DF}} - \epsilon_{\text{SGS}}^{\text{LES}}\rangle / \langle \epsilon_{\text{SGS}}^{\text{LES}}\rangle \tag{21}$$

of order 18% for the flow in Figs. 1–3. To reduce this error, a second iteration can be performed by using b_0 to compute the tensor R_{ij} in Eq. (13) and subsequently solving the elliptic differential equation (12) for the tensor $\mathcal{T}_{ij}^{\mathrm{DF}}$. Upon updating β_{ij} in Eq. (19) with the resulting $\mathcal{T}_{ij}^{\mathrm{DF}}$, a positive root b_1 is obtained by solving Eq. (17) again. After two iterations, error values of order 2% are observed in the simulations, as shown in Fig. 4(a), which indicates that the iterative method converges rapidly. Nonetheless, Fig. 4(b) shows that the values b_0 and b_1 are of similar order despite the reduction in the relative error. This two-step iterative procedure is adopted in the simulations presented below.

B. Dynamic procedure based on kinetic-energy matching [LES-DF(k) procedure]

An alternative and simpler dynamic procedure, referred to as LES-DF(k), can be formulated by constraining the SGS kinetic energy from the DF model, $k_{\mathrm{SGS}}^{\mathrm{DF}} = \mathcal{T}_{kk}^{\mathrm{DF}}/2$, to be equal to the one calculated from the LES model, $k_{\mathrm{SGS}}^{\mathrm{LES}} = \mathcal{T}_{kk}^{\mathrm{LES}}/2$, where $\mathcal{T}_{kk}^{\mathrm{DF}}$ is given by Eq. (14). Substitution of the consistency requirement $k_{\mathrm{SGS}}^{\mathrm{DF}} = k_{\mathrm{SGS}}^{\mathrm{LES}}$ into Eq. (12) leads to the expression

$$\mathcal{T}_{kk}^{\mathrm{LES}} - b^2 \frac{\partial^2 \mathcal{T}_{kk}^{\mathrm{LES}}}{\partial x_\ell \partial x_\ell} - 2b \frac{\partial b}{\partial x_m} \frac{\partial \mathcal{T}_{kk}^{\mathrm{LES}}}{\partial x_m} = R_{kk}, \tag{22}$$

where R_{kk} is given in Eq. (13).

Equation (22) is a nonlinear partial differential equation that provides the spatial distribution of b. If b is assumed to be spatially uniform, as done in the simulations presented below, a much simpler volume-averaged version of Eq. (22) has to be solved, namely,

$$\langle\alpha\rangle b^4 + \langle\beta\rangle b^2 - \langle\gamma\rangle = 0, \tag{23}$$

where the coefficients α, β and γ are given by

$$\alpha = \frac{\partial^2 \overline{u}_k}{\partial x_\ell \partial x_\ell} \frac{\partial^2 \overline{u}_k}{\partial x_m \partial x_m}, \tag{24}$$

$$\beta = 2 \frac{\partial \overline{u}_k}{\partial x_\ell} \frac{\partial \overline{u}_k}{\partial x_\ell} + \frac{\partial^2 \mathcal{T}_{kk}^{\mathrm{LES}}}{\partial x_\ell \partial x_\ell}, \tag{25}$$

$$\gamma = \mathcal{T}_{kk}^{\mathrm{LES}}, \tag{26}$$

with $b^2 > 0$ corresponding to the physically relevant root. In triply-periodic flows, the volume average of the coefficient β in Eq. (25) simplifies to $\langle\beta\rangle = 2\epsilon_r/\nu$, where $\epsilon_r = \langle\nu(\partial \overline{u}_k/\partial x_\ell)(\partial \overline{u}_k/\partial x_\ell)\rangle$ is the resolved dissipation. Note that there is no approximation required in order to enforce the consistency condition for the SGS kinetic energies, which is satisfied exactly. The same method has been extended to model unfiltered scalars in LES by imposing consistency in the subgrid variance [34].

In the simulations performed in this study, the SGS dissipation-matching and kinetic-energy-matching dynamic approaches described above lead to similar values of the coefficient b, as shown in the time series in Fig. 4(b). It is worth mentioning that Eqs. (17) and (23) yielded only one single positive root $b^2 > 0$ during the computations. Additionally, the resulting mean values of b correspond to differential filters with the same second moment as a spherical top-hat filter of radius $1.4\Delta - 1.5\Delta$, which suggests that the dynamic procedures yield realistic values of the effective filter width.

Spatially varying coefficients b could be computed, in a first approximation, by solving the biquadratic equations (17) or (23) locally in space without the volume-averaging operators, which are equivalent to Eqs. (16) or (22) when the gradients of b are neglected. It is noteworthy that the LES-DF(k) dynamic procedure yields $b = 0$ in the limit $\gamma \to 0$, as in regions close to the wall in wall-resolved LES of channel flows where the SGS model for the particles would automatically become deactivated. However, it should be stressed that it is only when b is spatially uniform, as in the cases addressed below, that the DF-modeled velocity field (6) is guaranteed to be incompressible. Computations with spatially varying b deserve further assessment and are deferred to future work.

IV. MODEL PERFORMANCE

The focus of this section is on examining the performance of the proposed LES-DF model in predicting dispersed-phase statistics. A description of the computational setup is given first, followed by an account of the main results.

A. Computational setup

Results are presented below in Secs. IV B 1–IV B 3 for DNS, LES with the resolved velocity $\overline{u}_i$ used in place of the unfiltered velocity u_i in Eq. (2), and LES with the DF-modeled velocity (6) used for u_i instead. In the notation, the acronyms LES-DF(ϵ) and LES-DF(k) indicate that the coefficient b, which is assumed to be spatially uniform, is obtained through the procedure described in Secs. III A [Eq. (17)] and III B [Eq. (23)], respectively. The computations involve numerical integrations of the mass and momentum conservation equations (3) and (4) in a triply-periodic domain. The baseline Reynolds number based on the Taylor microscale is $Re_\lambda = 85$. The calculations are conducted on staggered, uniform Cartesian grids of 256^3 points for DNS and 32^3 points for LES. These grids translate into maximum resolutions $\kappa_{max}\ell_k = 1.6$ and 0.2, respectively, where κ_{max} is the largest wavenumber resolved by the grid and $\ell_k = (\nu^3/\epsilon)^{1/4}$ is the Kolmogorov length.

Additional DNS and LES results at larger Re_λ and higher resolutions are reported in Sec. IV B 5 in a supporting role to address the behavior of the SGS particle model in a broader range of parameters. These cases are computed at $Re_\lambda = 136$ with 512^3 grid points for DNS ($\kappa_{max}\ell_k = 1.6$) and both 128^3 and 64^3 grid points for LES ($\kappa_{max}\ell_k = 0.4$ and 0.2, respectively).

Constant kinetic-energy linear forcing is applied in the momentum equation (4) to sustain the turbulence and compute stationary statistics (see Ref. [38] for details). In order to account for the unresolved portion of the energy that is not captured in LES, the values of the resolved kinetic energy injected in the LES correspond to 82% (for the 32^3 grid, $Re_\lambda = 85$ case), 90% (for the 64^3 grid, $Re_\lambda = 136$ case), and 96% (for the 128^3 grid, $Re_\lambda = 136$ case) of the corresponding DNS kinetic energy. This resolved energy is obtained by filtering the DNS with a box filter that has a filter width equal to the LES grid spacing Δ.

The numerical scheme consists of finite-difference energy-conserving discretizations of second-order central in space and fourth-order Runge-Kutta in time [39]. In order to integrate the particle equation of motion, the carrier-phase velocity is interpolated at the particle position using a trilinear interpolation. Higher-order interpolation schemes were employed, but they did not show any substantial modification of the results.

Once the flow has reached a statistically steady state, $N_p = 5 \times 256^3$ and 5×512^3 particles are randomly seeded in all the $Re_\lambda = 85$ and $Re_\lambda = 136$ cases, respectively. In order to study the performance of the DF model in predicting the DNS particle-concentration spectra, an Eulerian number-density field n is calculated in all cases by projecting the Lagrangian particles onto the nearest DNS grid point. Data collection starts once a sufficiently long time compared to the particle relaxation time t_a has passed after seeding the particles. Ensemble-averaged statistics are extracted from ten snapshots recorded during $16t_\ell$, where $t_\ell = \ell/u_\ell$ is the integral time computed with the integral length ℓ and velocity u_ℓ. The characteristic Stokes number

$$St_k = t_a/t_k \tag{27}$$

ranges from 0.1 to 10 in the simulations, with $t_k = \ell_k^2/\nu$ being the Kolmogorov turnover time. This corresponds to SGS Stokes numbers in the range

$$St_{SGS} = (\ell_k/\Delta)^{2/3} St_k \sim 0.02\text{–}2 \tag{28}$$

for all LES cases, where use of Kolmogorov scaling has been made in order to rewrite Eq. (5) in the form (28).
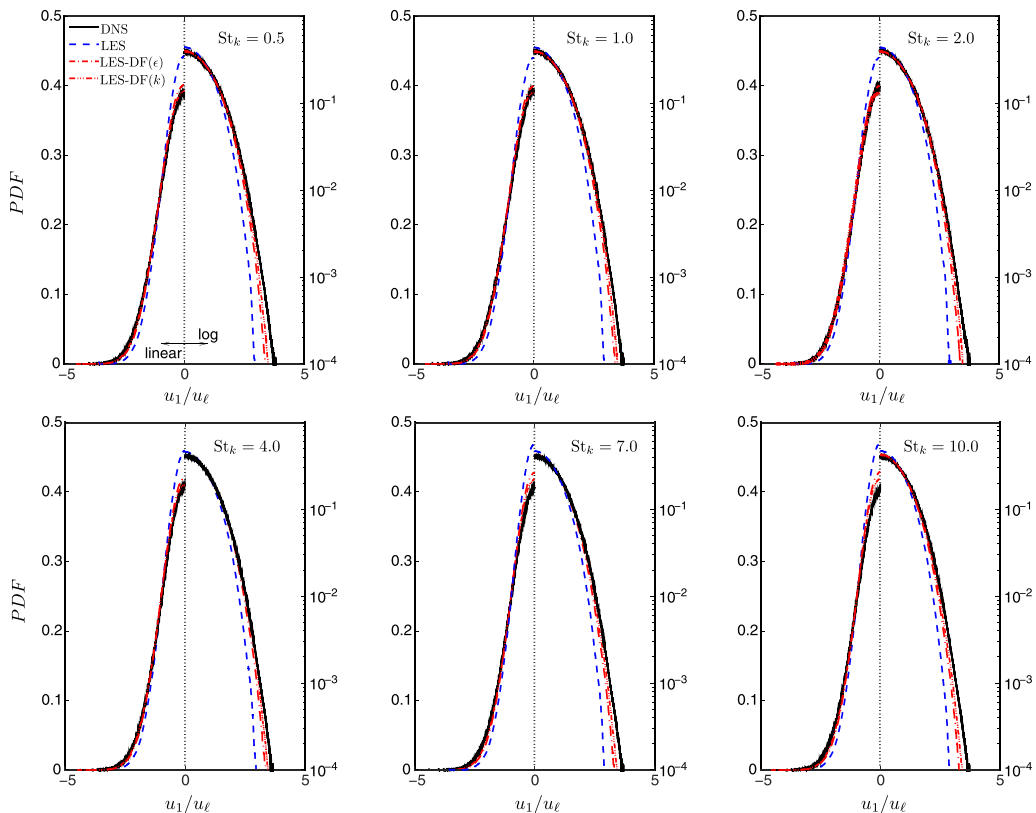
FIG. 5. DNS (256^3 grid points), LES (32^3 grid points) and the LES-DF model (32^3 grid points) normalized ensemble-averaged PDFs of the carrier-phase velocity component u_1 interpolated at the particle position for $Re_\lambda = 85$ and different Stokes numbers (see the legend in the top left panel for line types). The PDFs are symmetric with respect to $u_1 = 0$. Linear and logarithmically transformed PDFs are provided on each horizontal semiaxis to improve visualization of results.

In these computations, the SGS stress tensor $\mathcal{T}_{ij}^{\text{LES}}$ is calculated using the dynamic Smagorinsky (DS) model [40,41] along with the least-squares approach in Ref. [42] for the determination of the dynamic constants. Yoshizawa's closure for the SGS kinetic energy, with the model constant obtained dynamically from the DS model as in Ref. [41], is employed for the LES-DF computations when the kinetic-energy matching dynamic procedure in Sec. III B is used to determine b. Additional computations were performed using the minimum-dissipation (MD) model [43]. However, since MD does not yet provide a closure for the SGS kinetic energy, the Yoshizawa constant was also determined by the dynamic procedure of Ref. [41]. Although the predictive capabilities are enhanced near the LES cutoff when the MD model is used, no significant differences were observed in the dispersed-phase statistics with respect to the ones obtained using the DS model, except for particular aspects pointed out in Sec. IV B 4 that are related to preferential-concentration metrics at the upper end of the range of Stokes numbers explored here, when particles interact predominantly with near-cutoff eddy scales. Note that the change of model for the SGS stress $\mathcal{T}_{ij}^{\text{LES}}$ requires no modifications in the formulation of the dynamic procedures presented in Sec. III.

The ensemble-averaged dispersed-phase statistics analyzed below include PDFs of the carrier-phase velocity at the particle position, along with PDFs of particle acceleration, Fourier spectra of the energy of the particle concentration fluctuations, and radial distribution functions (RDFs). Formal explanations of these standard metrics can be found elsewhere [6,7,20].
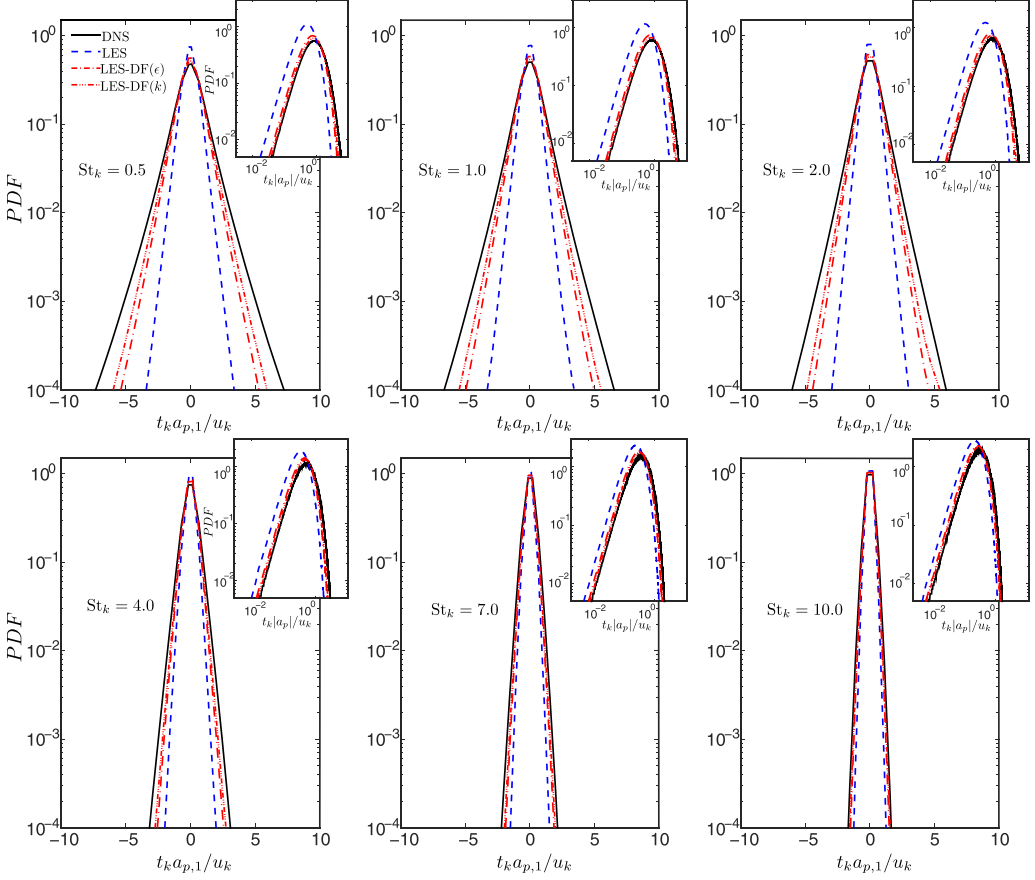
FIG. 6. DNS (256^3 grid points), LES (32^3 grid points), and the LES-DF model (32^3 grid points) normalized ensemble-averaged PDFs of particle-acceleration component $a_{p,1}$ and particle-acceleration vector magnitude $|a_p|$ (insets) for $Re_\lambda = 85$ and different Stokes numbers (see the legend in the top left panel for line types).

B. Discussion of results

1. Carrier-phase velocity sampled by particles

The prediction of the PDF of the carrier-phase velocity sampled by the particles is considerably improved with the LES-DF model, particularly with the kinetic-energy-matching dynamic procedure [LES-DF(k)], as shown in Fig. 5. The PDF of this quantity is computed by creating a histogram upon collecting the carrier-phase velocity vector u_1 interpolated at all positions of all particles during their flight trajectories. For tracers and very heavy particles, the DNS PDFs resemble, respectively, those of the Lagrangian and Eulerian carrier-phase velocities, both characterized by nearly Gaussian flatness factors $F \sim 3.0$ since the tails of the distributions correspond to large-scale-eddy motions.

The utilization of the LES-DF method leads to flatness factors of the carrier-phase velocity sampled by the particles closer to DNS. For instance, for $St_k = 0.1$, the PDF predicted by DNS has a flatness $F = 2.86$, while LES-DF(k) predicts $F = 2.81$. These are in contrast to the smaller value $F = 2.76$ obtained from LES without a model for the SGS velocity. Improved predictions are also observed in the central region of the PDFs, which corresponds to velocities of small-scale eddies sampled by particles. The same trends are observed for all tested Stokes numbers.
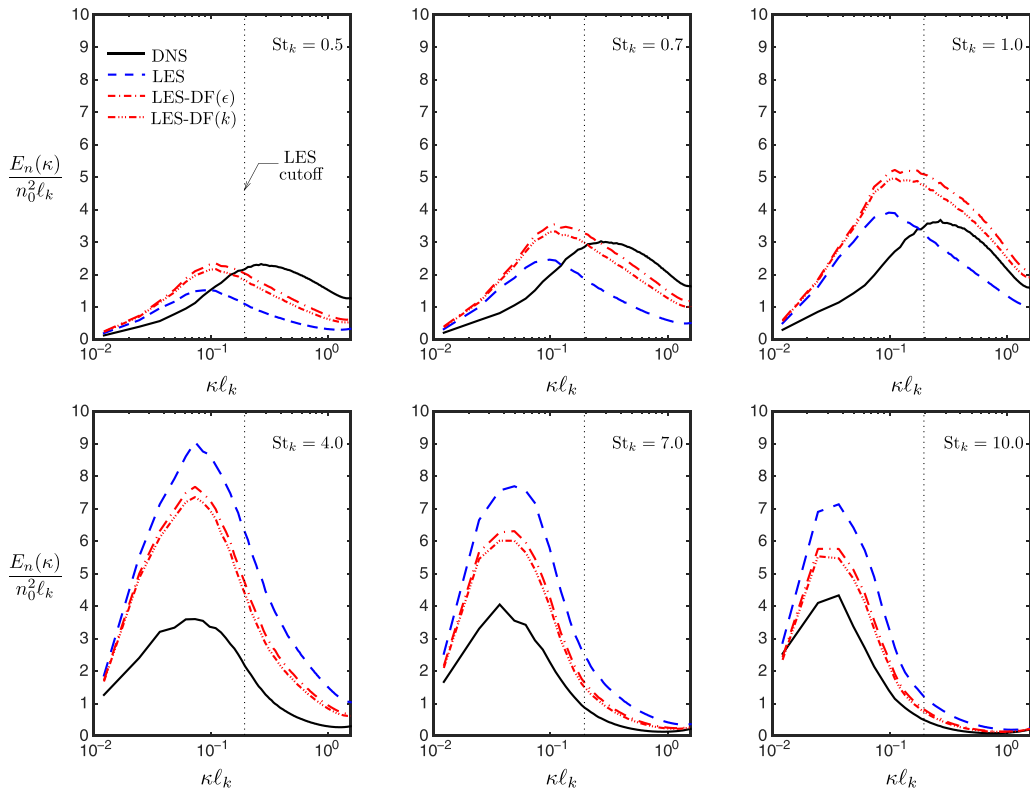
FIG. 7. DNS (256^3 grid points), LES (32^3 grid points), and the LES-DF model (32^3 grid points) ensemble-averaged particle concentration spectra for $\mathrm{Re}_\lambda = 85$ and different Stokes numbers (see the legend in the top left panel for line types).

2. Particle acceleration

The LES-DF model yields enhanced results for the PDF of the particle-acceleration component $a_{p,1} = (4/3)\pi\rho_p a^3 (du_{p,1}/dt)$ and for the particle-acceleration vector magnitude $|a_p|$, as observed in Fig. 6. The increased intermittency introduced by the DF-modeled SGS velocity, shown in Figs. 2 and 3, translates into results closer to DNS by creating longer tails in the PDFs of $a_{p,1}$. The top row in Fig. 6 shows that the improvement becomes particularly visible at small Stokes numbers, where the particles are subject to the accelerations caused by the small-scale rapidly turning eddies that are not captured in LES but are only partially modeled in the LES-DF approach, so the likelihood of the particles having large accelerations is significantly increased and shifted toward the DNS. For instance, for $\mathrm{St}_k = 2.0$, the flatness of the PDF of $a_{p,1}$ predicted by LES is $F = 4.27$, while LES-DF(k) gives $F = 4.78$, the latter being closer to the DNS value $F = 5.16$.

In connection with the improved predictions of $a_{p,1}$ is the much better agreement with the DNS PDFs of the particle-acceleration vector magnitude $|a_p| = (a_{p,i}a_{p,i})^{1/2}$ when the LES-DF model is used, as shown in the insets in Fig. 6. In the absence of subgrid intermittency, LES without model for SGS velocity fluctuations leads to underprediction of $|a_p|$, particularly at small Stokes numbers where the particles become tracers of a large portion of the small eddies. On the other hand, utilization of the LES-DF method shifts the maximum-probability peak of $|a_p|$ toward larger values, leading to a remarkable match with the DNS PDFs. A general conclusion observed here with regard to particle acceleration is that the kinetic-energy matching dynamic procedure of Sec. III B leads to more accurate predictions in comparison with the dissipation-matching one. Additional statistics regarding particle kinematics, such as the mean curvature angle of the particle trajectories, have been
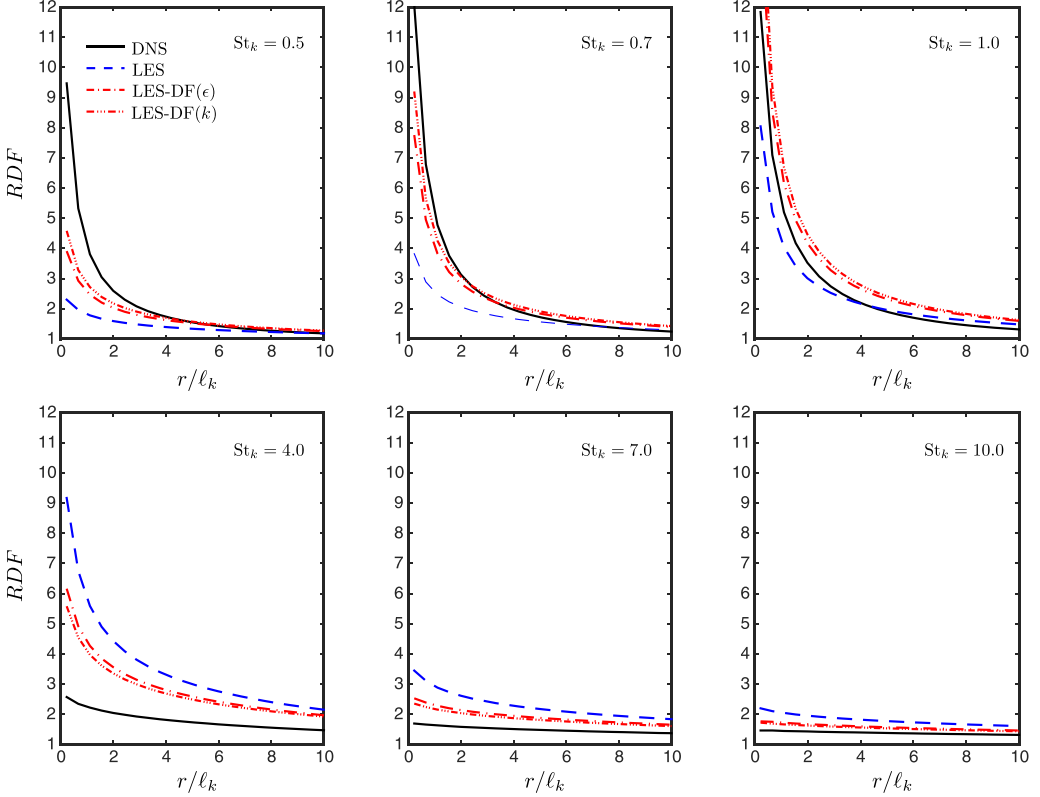
FIG. 8. DNS (256^3 grid points), LES (32^3 grid points), and the LES-DF model (32^3 grid points) ensemble-averaged radial distribution functions for $Re_\lambda = 85$ and different Stokes numbers (see the legend in the top left panel for line types).

shown in a recent study (see Fig. 3 in Ref. [44]) to be correctly recovered by the LES-DF model presented here.

3. Preferential concentration

The results presented above for the particle acceleration statistics depend only weakly on localized turbulence phenomena, in that extreme particle accelerations are achievable by simply augmenting the carrier-phase velocity sampled by the particles with large fluctuations. In principle, such externally imposed fluctuations do not need to be correlated with the resolved dynamics of turbulence structures. They may be modeled in the particle frame as random time-dependent disturbances of u_i in Eq. (2) that induce rare events that increase the flatness of the acceleration distribution, as in stochastic modeling [20]. This approach, however, is incapable of predicting other types of phenomena that largely depend on spatially localized turbulence dynamics, such as the preferential concentration of particles [45,46]. In preferentially concentrated regimes (i.e., $St_k \sim 1$), the particles move with the large eddies while slipping on the small ones, which are known to bear the highest internal intermittency of vorticity and strain rate. In this way, the particles are centrifuged from small intense vortices and accumulate in interstitial strained regions giving rise to characteristic filamentous zones where the number density of particles is large compared to the mean.

It is noteworthy that the DF-modeled SGS velocity (7) requires spatially localized information of the resolved field and therefore has some potential to reverse the erroneous trends observed in preferential-concentration metrics computed from LES. Figure 7 shows the Fourier energy spectra E_n
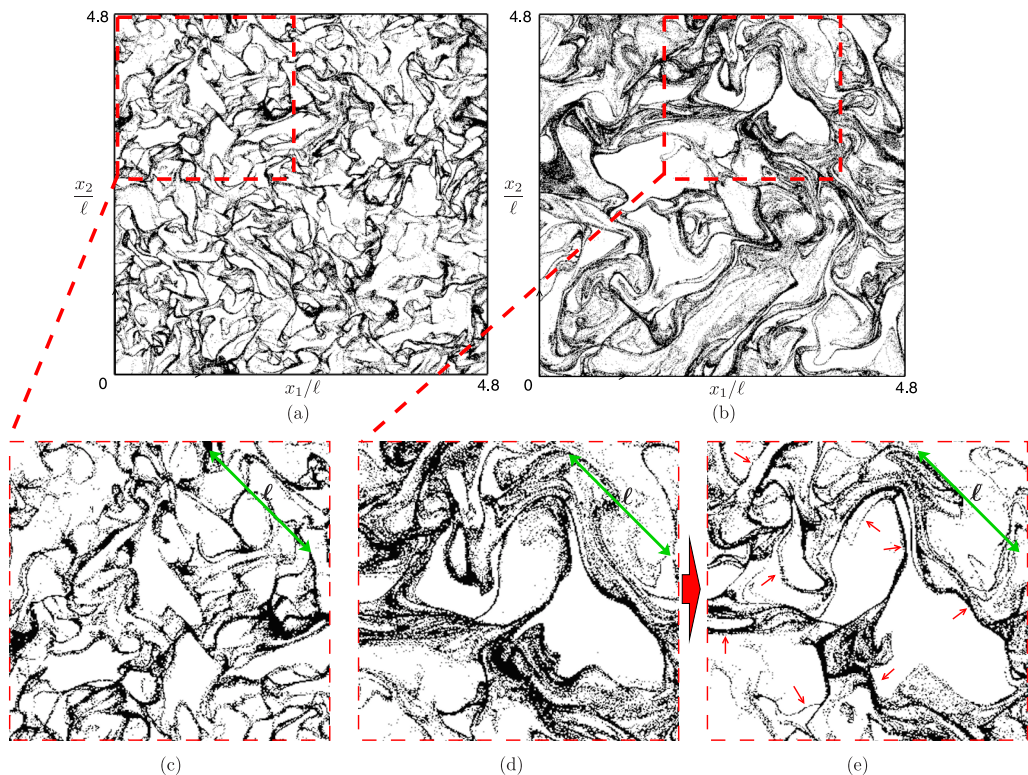
FIG. 9. Instantaneous spatial distribution of particles (dots) contained in an x_3 slice of thickness $2\ell_k$ for $St_k = 1$ and $Re_\lambda = 85$ including (a) DNS (256^3 grid points), (b) LES (32^3 grid points), (c) DNS (zoomed area), (d) LES (zoomed area) and (e) the LES-DF model resulting particle distributions in the same region. The double-ended arrows in (c)–(e) indicate the integral length ℓ. Panels (d) and (e) correspond to solutions evaluated at the same time instant $t/t_\ell = 19$ starting from the same initial conditions. The DF-model constant b is obtained using the dynamic procedure in Sec. III B.

of the particle-concentration spatial fluctuations relative to the mean. Specifically, Fig. 7 quantifies the characteristic scales and spectral intensities associated with the structures of the number-density field n. In particular, the DNS spectra show that the wavenumber of the peak spectral intensity decreases with increasing St_k, while the variance of n (i.e., the integral of the spectrum) evolves nonmonotonically with St_k and reaches a maximum at $St_k \sim 1$. This is in agreement with known dynamics by which the preferential-concentration effect in homogeneous-isotropic turbulence is most intense when $St_k \sim 1$, causing accumulation of particles in small-scale structures that lead to maximum spatial variance of n. The LES without model for the SGS velocity, on the other hand, underpredicts the peak wavenumber for $St_k \lesssim 1$, thereby indicating that the characteristic sizes of the most energetic structures of n are vastly larger than in DNS. It also overpredicts the energy associated with those structures for $St_k > 1$.

A similar problem is observed in Fig. 8 for RDFs, which quantify the likelihood of finding particles at a radial distance r from a test particle. Specifically, LES without a model for the SGS velocity underpredicts the RDF for $St_k \lesssim 1$ and overpredicts it for $St_k > 1$. These findings suggest that LES yields accumulation of particles in too long and slender zones for $St_k \lesssim 1$. Conversely, LES predicts the correct characteristic size of accumulation zones yet with excessive concentration of particles with respect to DNS when $St_k > 1$. These erroneous LES behaviors can be easily illustrated in physical space for $St_k = 1.0$, as done in Figs. 9(a)–9(d). The size of the accumulation zones predicted by LES can be visually correlated with those
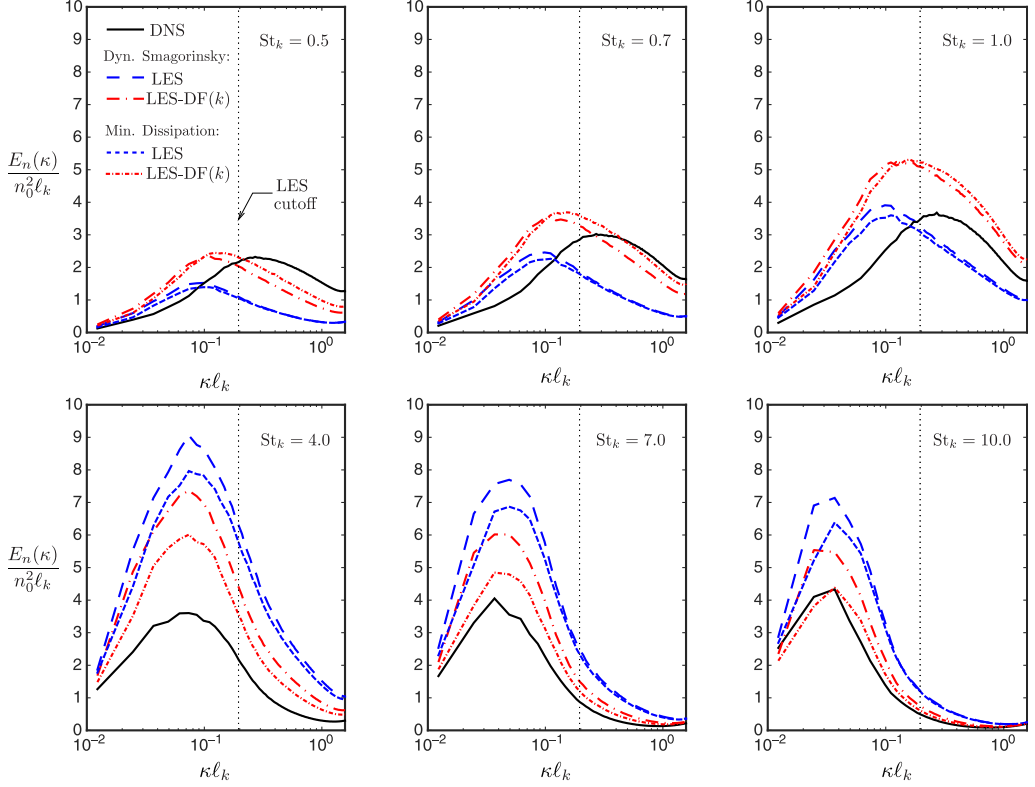
FIG. 10. Sensitivity of LES (32^3 grid points) and the LES-DF model (32^3 grid points) ensemble-averaged particle concentration spectra to carrier-phase SGS stress model choice (i.e., dynamic Smagorinsky versus minimum-dissipation model) for $Re_\lambda = 85$ and different Stokes numbers (see the legend in the top left panel for line types).

of the flow structures shown in Fig. 3(b), which lack the small-scale spatial intermittency necessary to cause accumulation of particles in the much shorter and spottier filaments observed in DNS.

The utilization of the LES-DF model proposed here, which injects spatial intermittency in the number density n through the modeled SGS velocity u_i', shifts the peak wavenumber of the spectra E_n in Fig. 7 toward higher DNS-like values for $St_k \lesssim 1$ and decreases the excess in particle-concentration energy for $St_k > 1$. Similarly, the LES-DF model generally corrects the erroneous trends of LES for the RDF while maintaining the nonmonotonic behavior with respect to St_k. However, it should be emphasized that the SGS velocity u_i' does not contain turbulence structures smaller than the grid size, as described in Sec. II. Therefore, although the overall results are clearly improved with the utilization of the model, the capabilities of the LES-DF model to recover the DNS preferential-concentration statistics are limited, as evidenced in Figs. 7 and 8. In all cases, the dynamic procedure based on kinetic-energy matching yields the best model performance.

An interesting case for illustrating the action of the DF model is that of $St_k = 1$ shown in Fig. 9(e), which indicates that the model acts to antidisperse the particles generating sharper filaments with higher concentration [see red arrows in Fig. 9(e)] but of roughly the same scale as in LES, in agreement with the statistical quantifications shown in Figs. 7 and 8 (top right panels). A model aimed at fully matching DNS scales and concentration energies of the particle clouds requires physics-based regeneration of turbulence over an extended range of wavenumbers beyond the grid cutoff. Such regeneration of the subgrid scales cannot be achieved with the present model, which
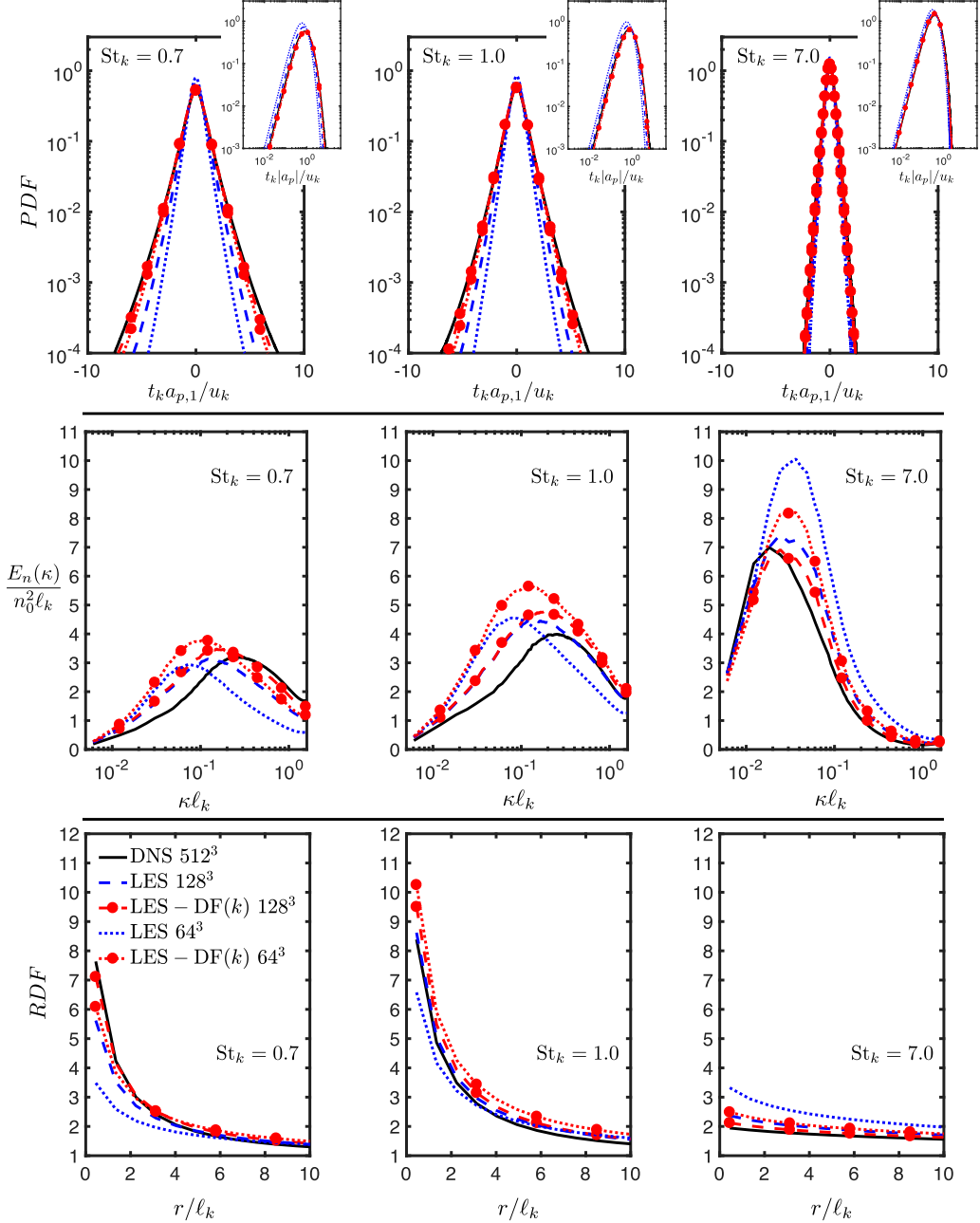
FIG. 11. LES-DF model performance at larger Reynolds number $\mathrm{Re}_\lambda = 136$ and different resolutions (see the legend in bottom left panel). The figure shows ensemble-averaged values of particle acceleration (top row), particle concentration spectra (middle row), and RDF (bottom row) for three different Stokes numbers (columns).

is intrinsically limited to scales near the grid cutoff, and must involve the study of local turbulence characteristics sampled by the particle clouds, perhaps using spatially localized basis functions such as wavelets [47,48].

4. Effects of the SGS model for the carrier-phase stress

An enhancement in predictions of particle accumulation can be achieved with the LES-DF model using the MD model for the SGS stress tensor of the carrier phase [43], but such improvement is only noticeable at relatively large Stokes numbers, as shown in Fig. 10 (bottom row). In this range of St_k values, the particles interact predominantly with the near-cutoff eddies, as indicated by the near-unity values of the associated SGS Stokes number (i.e., $St_{SGS} = 0.6$ for $St_k = 4.0$, $St_{SGS} = 1.1$ for $St_k = 7.0$, and $St_{SGS} = 1.6$ for $St_k = 10.0$). Since the MD model is less dissipative than the DS and is known to capture more accurately the turbulent eddies near the grid cutoff [43], an improved match with the DNS concentration spectra is achieved, particularly at $St_k = 10$ (see Fig. 10, bottom right panel). Similar improvements are found in the RDF statistics. These considerations illustrate the relevance of the model for the SGS stress tensor of the carrier phase in predicting spatial distributions of particles in regimes when they interact most intensely with turbulence scales near the grid cutoff, particularly in computations performed on coarse grids such as the ones presented here.

5. Effects of the Reynolds number and grid resolution

Figure 11 shows the performance of the LES-DF model compared to DNS and LES at higher Reynolds numbers and different grid resolutions. A number of general conclusions can be extracted from these results. As expected, the agreement between LES and DNS improves as the LES grid resolution increases. Additionally, that increment of LES grid resolution results in a diminishing relevance of the model since there is less fluctuation in the subgrid scales and the dynamic model coefficient b becomes correspondingly smaller. Remarkably, the LES-DF model is able to largely improve the dispersed-phase statistics predicted by LES on a 64^3 grid. For instance, the LES-DF model on a 64^3 grid produces better predictions for particle acceleration and RDF statistics than those obtained from LES on a 128^3 grid. Similarly, in all cases the model corrects the spurious trends caused by LES on the concentration spectra that were discussed in Sec. IV B 3.

V. CONCLUSIONS

A dynamic model for LES of particle-laden turbulence has been proposed in this study. The model formulation is relatively simple, does not entail any significant computational overhead, and is flexible enough to be deployed in any type of flow solvers and grids, including unstructured setups. The model is based on elliptic differential filters. The only model parameter, which is related to the effective filter width, is determined dynamically by imposing consistency constraints in the subgrid energetics. Therefore, no tuning of parameters is required. Two different dynamic procedures were described, one based on matching the dissipation provided by the model with that of the model used for the SGS stress tensor of the carrier phase and another one based on matching their SGS kinetic energies. Throughout the computations, it was observed that the latter procedure consistently yields the best agreement with DNS. In particular, the performance of the model was tested in LES of homogeneous-isotropic turbulence laden with particles, where improved agreement with DNS was observed in the dispersed-phase statistics for a wide range of Stokes numbers, including particle acceleration, local carrier-phase velocity, particle-concentration energy spectra, and RDFs.

There are several aspects that are worthy of further investigation. For instance, particle collisions and two-way coupling effects have been neglected in these computations, although the probability of collisions and the mass loading may be significantly increased within the clouds of preferentially concentrated particles. In principle, a collision model can be incorporated in Eq. (2) that does not require subgrid-scale modeling. Note, however, that the correct prediction of the RDF and number-density distribution statistics, or equivalently of preferential-concentration physics, are important for the quantification of collisions [6,7]. Similarly, the two-way coupling force on the gas largely depends on the position and acceleration of the particles [49]. The fact that improvements are observed in all

of the aforementioned statistics when the DF model is used suggests that its characteristics may be beneficial for the prediction of these processes in LES.

The subgrid model that has been described here transcends particle-laden flows and may be employed in other types of problems in LES that require modeling for the SGS velocity. These relate to relevant applications in two-phase flows such as liquid-gas interface modeling [50], in which an SGS velocity is used to model interface distortion and breakup, and in chemically-reacting flows, where the utilization of an SGS velocity model is central to the quantification of small-scale flame corrugations leading to a deflagration-to-detonation transition [51].

ACKNOWLEDGMENTS

[1] A. L. Sánchez, J. Urzay, and A. Liñán, The role of separation of scales in the description of spray combustion, Proc. Combust. Inst. **35**, 1549 (2015).

[2] J. Urzay, M. Bassenne, G. I. Park, and P. Moin, *Characteristic Regimes of Subgrid-Scale Coupling in LES of Particle-Laden Turbulent Flows*, Annual Research Briefs 2014, Center for Turbulence Research (Stanford University, Stanford, 2014), pp. 3–13.

[3] V. Armenio, U. Piomelli, and V. Fiorotto, Effect of the subgrid scales on particle motion, Phys. Fluids **11**, 3030 (1999).

[4] J. G. M. Kuerten and A. Vreman, Can turbophoresis be predicted by large-eddy simulation? Phys. Fluids **17**, 011701 (2005).

[5] C. Marchioli, M. Salvetti, and A. Soldati, Some issues concerning large-eddy simulation of inertial particle dispersion in turbulent bounded flows, Phys. Fluids **20**, 040603 (2008).

[6] G. Jin, G. W. He, and L. P. Wang, Large-eddy simulation of turbulent collision of heavy particles in isotropic turbulence, Phys. Fluids **22**, 055106 (2010).

[7] B. Ray and L. R. Collins, Preferential concentration and relative velocity statistics of inertial particles in Navier-Stokes turbulence with and without filtering, J. Fluid Mech. **680**, 488 (2011).

[8] M. J. Cernick, S. W. Tullis, and M. F. Lightstone, Particle subgrid scale modeling in large-eddy simulations of particle-laden turbulence, J. Turbul. **16**, 101 (2014).

[9] G. He, G. Jin, and Y. Yang, Space-time correlations and dynamic coupling in turbulent flows, Annu. Rev. Fluid Mech. **49**, 51 (2017).

[10] A. D. Gosman and E. Ioannides, Aspects of computer simulation of liquid-fueled combustors, J. Energy **7**, 482 (1983).

[11] Q. Wang and K. Squires, Large eddy simulation of particle-laden turbulent channel flow, Phys. Fluids **8**, 1207 (1996).

[12] K. Fukagata, S. Zahrai, and F. H. Bark, Dynamics of Brownian particles in a turbulent channel flow, Heat Mass Transfer **40**, 715 (2004).

[13] B. Shotorban and F. Mashayek, A stochastic model for particle motion in large-eddy simulation, J. Turbul. **7**, N18 (2006).

[14] P. Fede, O. Simonin, P. Villedieu, and K. Squires, Stochastic modeling of the turbulent subgrid fluid velocity along inertial particle trajectories, *Proceedings of the Summer Program, Center for Turbulence Research* (Stanford University, Stanford, 2006), pp. 247–258.

[15] A. Berrouk, D. Laurence, J. Riley, and D. Stock, Stochastic modeling of inertial particle dispersion by subgrid motion for LES of high Reynolds number pipe flow, J. Turbul. **8**, N50 (2007).

[16] M. Bini and W. Jones, Particle acceleration in turbulent flows: a class of nonlinear stochastic models for intermittency, Phys. Fluids **19**, 035104 (2007).

[17] J. Pozorski and S. Apte, Filtered particle tracking in isotropic turbulence and stochastic modeling of subgrid-scale dispersion, Int. J. Multiphase Flow **35**, 118 (2009).

[18] G. Jin and G. He, A nonlinear model for the subgrid timescale experienced by heavy particles in large eddy simulation of isotropic turbulence with a stochastic differential equation, New J. Phys. **15**, 035011 (2013).

[19] M. Gorokhovski and R. Zamansky, Lagrangian simulation of large and small inertial particles in a high Reynolds number flow: Stochastic simulation of subgrid turbulence/particle interactions, *Proceedings of the Summer Program, Center for Turbulence Research* (Stanford University, Stanford, 2014), pp. 37–46.

[20] J. P. Minier, On Lagrangian stochastic methods for turbulent polydisperse two-phase reactive flows, Prog. Energy Combust. Sci. **50**, 1 (2015).

[21] B. Shotorban and F. Mashayek, Modeling subgrid-scale effects on particles by approximate deconvolution, Phys. Fluids **17**, 081701 (2005).

[22] J. G. M. Kuerten, Subgrid modeling in particle-laden channel flow, Phys. Fluids **18**, 025108 (2006).

[23] W. Michalek, J. Kuerten, J. Zeegers, R. Liew, J. Pozorski, and B. Geurts, A hybrid stochastic deconvolution model for large-eddy simulation of particle-laden flow, Phys. Fluids **25**, 123302 (2013).

[24] C. Gobert and M. Manhart, Subgrid modeling for particle-LES by spectrally optimised interpolation (SOI), J. Comput. Phys. **230**, 7796 (2011).

[25] B. Ray and L. R. Collins, A subgrid model for clustering of high-inertia particles in large-eddy simulations of turbulence, J. Turbul. **15**, 366 (2014).

[26] S. Murray, M. F. Lightstone, and S. Tullis, Single-particle Lagrangian and structure statistics in kinematically simulated particle-laden turbulent flows, Phys. Fluids **28**, 033302 (2016).

[27] J. Bardina, J. H. Ferziger, and W. C. Reynolds, *Improved Subgrid Scale Models for Large-Eddy Simulation*, Proceedings of the 13th Conference on Fluid and Plasma Dynamics, Snowmass, 1980 (AIAA, Reston, 1980), paper 80-1357.

[28] S. Liu, C. Meneveau, and J. Katz, On the properties of similarity subgrid-scale models and deduced from measurements in a turbulent jet, J. Fluid Mech. **275**, 83 (1994).

[29] A. W. Cook, Determination of the constant coefficient in scale similarity models of turbulence, Phys. Fluids **9**, 1485 (1997).

[30] M. Germano, Differential filters for the large-eddy numerical simulation of turbulent flows, Phys. Fluids **29**, 1755 (1986).

[31] M. Germano, Differential filters of elliptic type, Phys. Fluids **29**, 1757 (1986).

[32] S. Bose and P. Moin, A dynamic slip boundary condition for wall-modeled large-eddy simulations, Phys. Fluids **26**, 015104 (2014).

[33] G. I. Park, J. Urzay, M. Bassenne, and P. Moin, *A Dynamic Subgrid-Scale Model Based on Differential Filters for LES of Particle-Laden Turbulent Flows*, Annual Research Briefs 2015, Center for Turbulence Research (Stanford University, Stanford, 2015), pp. 17–26.

[34] M. Bassenne and J. Urzay, *A Dynamic Approximate Deconvolution Model for Unfiltered Scalars in LES*, Annual Research Briefs 2016, Center for Turbulence Research (Stanford University, Stanford, 2016), pp. 105–106.

[35] N. Okong'o and J. Bellan, A priori subgrid analysis of temporal mixing layers with evaporating droplets, Phys. Fluids **12**, 1573 (2000).

[36] S. Bose and P. Moin, Grid independent large-eddy simulation using explicitly filtering, Phys. Fluids **22**, 105103 (2010).

[37] N. Park and K. Mahesh, A velocity-estimation subgrid model constrained by subgrid scale dissipation, J. Comput. Phys. **227**, 4190 (2008).

[38] M. Bassenne, J. Urzay, G. I. Park, and P. Moin, Constant-energetics physical-space forcing methods for improved convergence to homogeneous-isotropic turbulence with application to particle-laden flows, Phys. Fluids **28**, 035114 (2016).

[39] H. Pouransari, M. Mortazavi, and A. Mani, *Parallel Variable-Density Particle-Laden Turbulence Simulation*, Annual Research Briefs 2015, Center for Turbulence Research (Stanford University, Stanford, 2015), pp. 43–54.

[40] M. Germano, U. Piomelli, P. Moin, and W. H. Cabot, A dynamic subgrid-scale eddy viscosity model, Phys. Fluids **3**, 1760 (1991).

[41] P. Moin, K. Squires, W. Cabot, and S. Lee, A dynamic subgrid scale model for compressible turbulence and scalar transport, Phys. Fluids **3**, 2746 (1991).

[42] D. K. Lilly, A proposed modification of the Germano subgridscale closure method, Phys. Fluids **4**, 633 (1992).

[43] W. Rozema, H. J. Bae, P. Moin, and R. Verstappen, Minimum-dissipation models for large-eddy simulation, Phys. Fluids **27**, 085107 (2015).

[44] B. Kadoch, M. Bassenne, M. Esmaily-Moghadam, K. Schneider, M. Farge, and W. J. T. Bos, Multi-scale geometrical Lagrangian statistics: Extensions and applications to particle-laden turbulent flows, *Proceedings of the Summer Program, Center for Turbulence Research* (Stanford University, Stanford, 2016), pp. 53–62.

[45] K. D. Squires and J. K. Eaton, Preferential concentration of particles by turbulence, Phys. Fluids **3**, 1169 (1991).

[46] A. Robinson, On the motion of small particles in a potential field of flow, Commun. Pure Appl. Math. **9**, 69 (1956).

[47] M. Bassenne, J. Urzay, and P. Moin, *Spatially-Localized Wavelet-Based Spectral Analysis of Preferential Concentration in Particle-Laden Turbulence*, Annual Research Briefs 2015, Center for Turbulence Research (Stanford University, Stanford, 2015), pp. 3–16.

[48] M. Bassenne, J. Urzay, and P. Moin, *Extraction of Coherent Clusters in Particle-Laden Turbulent Flows using Wavelet Filters*, Annual Research Briefs 2016, Center for Turbulence Research (Stanford University, Stanford, 2016), pp. 105–119.

[49] A. Ferrante and S. Elghobashi, On the physical mechanisms of two-way coupling in particle-laden isotropic turbulence, Phys. Fluids. **15**, 315 (2003).

[50] M. Herrmann and M. Gorokhovski, A large eddy simulation subgrid model for turbulent phase interface dynamics, *Proceedings of the 11th Triennial International Annual Conference on Liquid Atomization and Spray Systems (ICLASS 2009)* (Curran, Red Hook, 2009).

[51] F. Ciaraldi-Schoolmann, I. R. Seitenzahl, and F. K. Röpke, A subgrid-scale model for deflagration-to-detonation transitions in Type Ia supernova explosion simulations, Astron. Astrophys. **559**, A117 (2013).